Polym. Bull. (2011) 67:729–740
DOI 10.1007/s00289-011-0498-8

ORIGINAL PAPER

Dispersion and flame retardancy of ethylene vinylacetate/layered silicate nanocomposites using the masterbatch approach for cable insulating material

Jin Woo Bae · Tae Uk Yang · Gi Joon Nam · Gun Joo Lee · Byeong-Uk Nam · Jae Young Jho

Received: 29 July 2010 / Revised: 11 January 2011 / Accepted: 4 May 2011 /
Published online: 12 May 2011

Abstract Ethylene vinylacetate (EVA) copolymer-based nanocomposites with maleic anhydride-grafted ethylene-vinylacetate (EVAgMA) and organically modified clay (o-clay) were prepared in a twin screw extruder by following a two-step melt compounding method. EVAgMA/o-clay masterbatches with various clay contents up to 50 wt% were examined, after which the masterbatch with the highest clay content was melt compounded with EVA for the preparation of EVA/o-clay nanocomposites containing specific amounts of clay. Further morphological dispersion of the clay particles by highly polar EVA and shearing was confirmed in the EVA/o-clay nanocomposites by X-ray diffraction (XRD) and transmission electron microscopy (TEM). These morphologies led to increased thermal properties in air as well as a considerable decrease in heat release rate (HRR). EVA/o-clay/MDH nanocomposites were also prepared using a high clay-bearing masterbatch to confirm the synergistic flame retardancy of clay as a co-additive in EVA/MDH composites. EVA/o-clay/MDH nanocomposites prepared by substituting o-clay for MDH showed significantly lower and wider HRR during combustion compared to EVA/MDH composite.

J. W. Bae · T. U. Yang · J. Y. Jho (✉)
School of Chemical and Biological Engineering, Seoul National University,
Seoul 151-744, Korea
e-mail: jyjho@snu.ac.kr

G. J. Nam · G. J. Lee
Fundamental Technology Research Center, LS Cable Ltd. 555, Hogye-dong, Dongan-gu, Anyang-si,
Gyeonggi-do 431-080, Korea

B.-U. Nam (✉)
Department of Applied Chemical Engineering, Korea University of Technology and Education,
Chungnam 330–708, Korea
e-mail: bunam@kut.ac.kr

Keywords Ethylene vinylacetate · Maleic anhydride-grafted ethylene-vinylacetate · Masterbatch · Nanocomposite · Flame retardancy

Introduction

Polymer/layered silicate nanocomposites (PLSNs) have attracted a great deal of interest as a promising new kind of hybrid material ever since nylon-6/clay nanocomposites developed by the Toyota research group were found to have unexpected properties [1–3]. Compared to virgin polymer or conventional microcomposites, PLSNs based on organic–inorganic composites displayed outstanding physical properties such as moduli, strength, thermal resistance and fire retardance [4–10]. These advantages are supposedly due to the considerably large interfacial areas between the polymer and layered silicates, which have thicknesses of approximately 1 nm and very high aspect ratios (100–1000) and were exfoliated or intercalated throughout the polymer matrix [11, 12]. In general, PLSNs can be prepared by three different approaches: solution intercalation, in situ polymerization and polymer melt compounding. Among these, the melt compounding-intercalation method has been recognized as a promising approach for producing intercalated or exfoliated nanocomposites due to its environmentally friendly characteristics, versatility and industrial compatibility with conventional polymer-processing [13].

Ethylene vinylacetate (EVA) copolymers are widely used in a variety of fields, such as the cable and wire industries, because of both their excellent insulating abilities and favorable physical and chemical properties. In most cable applications, EVA needs to be compounded with a large amount of conventional inorganic filler, such as aluminum trihydroxide (ATH) or magnesium dihydroxide (MDH), to retard the flammability of EVA during combustion. However, many such inorganic fillers lead to dramatic decreases in both mechanical properties and processability [14].

To minimize these disadvantages, researchers have recently attempted to disperse EVA/layered silicate nanocomposites at the nanometer scale [15–17]. These layered silicates in EVA compounds have the ability to improve both thermal properties and flame retardancy due to the nanoscale dispersion of silicate platelets in the polymer matrix [16]. However, by the melt compounding method, completely exfoliated EVA/layered silicate nanocomposites cannot always be easily and reproducibly obtained due to decomposition and volatilization of the organic surfactants via Hoffmann elimination during the process [11, 16–21]. In addition, undesired protons on the clay surface are generated by the decomposition of surfactants, eventually causing the accelerated deacetylation of EVA. Taking these facts into account, EVA/layered silicate nanocomposites containing highly dispersed clay still cannot be made by the melt-mixing method. To overcome the limited dispersion of EVA/layered silicate nanocomposites, Jeon et al. [19] used maleic anhydride-grafted polyethylene as a compatibilizer, but only a partially exfoliated structure could be obtained Moreover, Shi et al. [22] recently developed exfoliated EVA/MMT nanocomposites using PVAc/MMT masterbatches, but this development was dependent upon the solution blending method.

To produce exfoliated EVA/layered silicate nanocomposites, we introduced a masterbatch system containing high content of o-clay and EVAgMA as a compatibilizer based on the melt compounding method. Subsequently, the masterbatch was simply melt-blended with EVA to produce EVA/layered silicate nanocomposites containing various amounts of clay. Clay dispersion, thermal stability, and flame retardancy of the nancomposites were investigated. Furthermore, to confirm the synergistic effect of partially replacing MDH with o-clay on flame retardancy, we prepared EVA/o-clay/MDH nanocomposites using the above-mentioned high clay content masterbatch.

Experimental

Materials

Ethylene vinylacetate containing 28% vinylacetate was purchased from DuPont Mitsui polychemical (Evaflex EVA421, melt flow rate of 4.0 g/10 min at 190 °C and 2.16 kg load, density of 0.95 g/mL). Maleic anhydride-grafted ethylene vinylacetate (EVAgMA, Fusabond MC 250D, melt flow rate of 1.4 g/10 min at 190 °C and 2.16 kg load, density of 0.96 g/mL) containing 28% vinylacetate and very high content of maleic anhydride was purchased from DuPont. Nanofil 5 o-clay, which was bentonite ion-exchanged with dimethyl distearyl ammonium chloride, was obtained from Sud-Chemie Clay Products. MDH was of high purity untreated grade (Magnifin H5), supplied by Martinswerk GmbH. Average particle size was 1.0 μm, and the specific surface area was 5.0 m^2/g. The o-clay and MDH were used after drying at 100 °C under vacuum conditions for 24 h without further treatment.

Preparation of EVAgMA/o-clay masterbatches

We prepared EVA-based nanocomposites according to a two-step melt compounding process. First, we prepared the EVAgMA/o-clay masterbatches. EVAgMA pellets were grinded into powder and dried in a vacuum oven for 24 h at 50 °C prior to manufacturing. The grinded EVAgMA and o-clay were uniformly pre-mixed with shaking in a PE-bag together with 0.2 wt% stabilizer. The mixtures were melt-mixed in a twin-screw extruder (Bautek Corp., $L/D = 40$, $\Phi = 19$ mm) operated at 130–200 °C and 150 rpm. The obtained strands were pelletized and then dried at 50 °C for 24 h in a vacuum oven. Compounding formulations of masterbatches are summarized in Table 1. (The sample names are abbreviated LMB-1 to -3.)

Table 1 Compounding formulations of EVAgMA/o-clay masterbatches

	EVAgMA	O-clay
LMB-1	90	10
LMB-2	70	30
LMB-3	50	50

Preparation of EVA/o-clay nanocomposites, EVA/MDH composite, and EVA/o-clay/MDH nanocomposites

After drying the masterbatches, the high clay content masterbatch and neat EVA pellets were pre-mixed with 0.2 wt% stabilizer in a PE-bag. The mixtures were melt compounded in the same twin-screw extruder at 130–200 °C and 200 rpm in order to obtain nanocomposite strands. The obtained strands were pelletized and then dried at 50 °C for 24 h in a vacuum oven. Their compounding formulations are listed in Table 2 (sample code LP-1 to -3).

The EVA/MDH composite was prepared in a mill roll mixer at a rotor speed of 100 rpm at 180 °C for 10 min. EVA/o-clay/MDH nanocomposites were compounded by partial substitution of MDH with 0, 2, 4 and 6 wt% o-clay in the same mill roll mixer at a rotor speed of 100 rpm at 180 °C for 10 min to confirm the synergistic flame retardancy between clay and MDH in the EVA matrix. The contents of all inorganic compounds in the EVA/o-clay/MDH nanocomposites were maintained at 60 wt%, whereas the concentrations of organic components remained the same. Their compounding formulations are listed in Table 2 (sample code LP-4 to -7).

Characterizations

The dispersion of layered silicates in the masterbatches and nanocomposites was investigated using a wide angle X-ray diffractometer (WAXD: D/MAX-IIIC) with Cu Kα radiation ($\lambda = 1.54$ Å) operated at 40 kV and 45 mA at room temperature. The diffractograms were scanned in 2θ ranges from 1.2 to 10° at a rate of 1°/min and with a step size of 0.01°. The basal spacing of layered silicates (d-spacing) was calculated by Bragg's law, $d = n\lambda/2\sin\theta$, based on the position of the (001) plane peak in the WAXD pattern.

The morphological structure of the EVA/o-clay nanocomposites was also obtained using a Carl Zeiss-LIBRA 120 Energy Filtering Transmission Electron Microscope (EF-TEM) operated at an accelerating voltage of 120 kV. Images were taken using a digital camera. Ultra-thin nanocomposites with thicknesses of 80 nm were ultramicrotomed using a Leica Ultracut UCT microtome at −100 °C, followed by transfer onto carbon-coated Cu grids of 200 mesh. The difference in electron

Table 2 Compounding formulations of EVA/o-clay nanocomposites (LP-1 to -3), EVA/MDH composite (LP-4) and EVA/o-clay/MDH nanocomposites (LP-5 to -7)

	LMB-3	EVA	EVAgMA	MDH
LP-1	4	96	–	
LP-2	10	90	–	
LP-3	20	80	–	
LP-4	–	34	6	60
LP-5	4	34	4	58
LP-6	8	34	2	56
LP-7	12	34	0	54

density between the layered silicates and polymer was sufficient for imaging. Thus, layered silicates appeared dark in bright-field TEM images.

The thermal stability of nanocomposites was investigated by thermogravimetric analysis (TGA, Perkin-Elmer). The analysis was carried out by heating samples from 30 to 600 °C under air flow at a heating rate of 10 °C/min.

Evaluations of flammability were measured using a Fire Testing Technology cone calorimeter of LS Cable Ltd., under ASTM E 1354-92. The testing sample was a 100 × 100 × 3 mm thick specimen prepared by compression molding at 180 °C under 15 metric tons of pressure. The samples were irradiated at a heat flux of 50 kW/m^2, after which the heat release rate (HRR) data were measured for the first 400 s. The exhaust gas flow was 24 L s^{-1}, and the spark was continuous until the sample ignited. The heat released was calculated from the consumption of oxygen due to combustion. The cone data reported here are the average of three replicated experiments.

Results and discussion

To improve the dispersion of o-clay in the EVA-based nanocomposite, melt compounding of the EVAgMA/o-clay masterbatch was conducted with increasing clay content up to 50 wt%; it was impossible to compound the masterbatch containing over 50 wt% clay content in the twin-screw extruder because the components were very immiscible, making it difficult to produce strands. The effect of the clay layers in the EVAgMA/o-clay masterbatches was evaluated using XRD and TGA.

Figure 1 displays the XRD patterns of the organically modified bentonite, Nanofil 5 (o-clay), and EVAgMA/o-clay masterbatches containing 10, 30, and 50 wt% o-clay content. The o-clay exhibited two well-defined diffraction peaks located around $2\theta = 3.02°$ and 6.97° that correspond to the basal interlayer spacing of 2.92 nm and 1.27 nm as determined by Bragg's equation. 2.92 nm ($2\theta = 3.02°$) is the mean interlayer spacing of the (001) plane ($d_{(001)}$) for the bentonite (001) reflection of dimethyl distearyl ammonium chloride, indicated by dotted line in Fig. 1. Also, 1.27 nm ($2\theta = 6.97°$) is original interlayer spacing for the layered silicates of bentonite. In the case of the EVAgMA/10 wt% o-clay masterbatch, there was no peak shown in the XRD pattern, thus indicating a fully exfoliated morphology due to the effects of strong hydrogen bonding between the polar functional group of EVAgMA and the hydroxy group of the silicates. When the clay concentration was gradually increased to 50 wt%, the reflection peak appeared at $2\theta = 2.15°$ ($d_{(001)} = 4.10$ nm), which corresponds to the distance between the (001) layered silicates in the EVAgMA matrix. Intercalation of the EVAgMA chains as a compatibilizer into the clay galleries seemed to occur based on the leftward peak shift. In addition, the other peaks at $2\theta = 4.29°$ and 6.44° also accompanied, while the (001) reflection peak of the layered silicates became stronger at the same diffraction angle. After calculation, the (002) and (003) plane reflections of the layered silicates in the EVAgMA matrix were confirmed. These results indicate the formation of ordered intercalated nanocomposite and coherent order of the silicate layers gradually increases with increasing clay content [23].

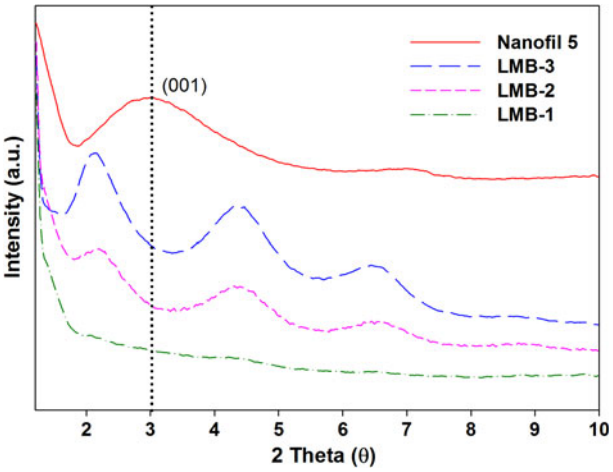

Fig. 1 XRD patterns of organically-modified bentonite, Nanofil 5 (o-clay) and EVAgMA/10, 30, 50 wt% o-clay masterbatches (LMB-1 to -3)

Figure 2 shows representative TGA curves for the EVAgMA/o-clay masterbatches containing 10, 30, and 50 wt% o-clay under air flow. In general, the TGA curves show that degradation of EVAgMA took place in two stages. The first (T_{d1}) onset decomposition temperature for the masterbatches was similar to that of EVAgMA, although T_{d1} gradually decreased as the content of o-clay in the masterbatch was increased. This is attributed to pyrolysis of the acetic ester groups of vinylacetate by the elimination of acetic acid [16]. There was also a second (T_{d2}) onset decomposition temperature. T_{d2} of the exfoliated masterbatch containing 10 wt% o-clay was highly retarded that of the intercalated masterbatches containing 30 and 50 wt% o-clay. Therefore, these results indicate that thermal degradation of the masterbatches was influenced by the degree of clay dispersion. Based on the

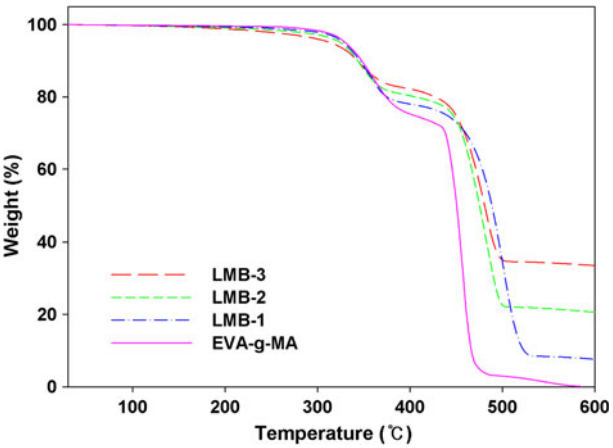

Fig. 2 TGA curves of EVAgMA and EVAgMA/10, 30, 50 wt% o-clay masterbatches (LMB-1 to -3)

XRD and TGA of the EVAgMA/o-clay masterbatches, the highest 50 wt% clay-contented masterbatch in this compounding process, although more deacetylation and partial exfoliation is shown, could be obtained and were expected to be used as a possible masterbatch for the preparation of the nanocomposites containing the desired amounts of clay.

Figure 3 compares the XRD patterns of the EVA/o-clay nanocomposites containing three different o-clay contents prepared from the EVAgMA/50 wt% o-clay masterbatch. No peaks in the 2θ range of 1.2–10° for 2, 5 wt% (low-contented) layered silicate in the EVA matrix were observed, which indicates homogenous exfoliated morphology. On the other hand, very wide and less intense peaks appeared at $2\theta = 4.15°$, 6.5° for the EVA/10 wt% o-clay nanocomposite, which implies the formation of an intercalated structure with a high degree of silicate–silicate interactions. These results show that highly dispersed EVA/o-clay nanocomposite prepared from high clay-contented masterbatch can be obtained by the dilution of polar EVA, by similar inherent polarities between the neat EVA and EVAgMA/o-clay masterbatch, and additional compounding.

To further confirm the dispersion state of clay in the matrix, TEM was carried out. Figure 4 presents the TEM images of EVA/5, 10 wt% o-clay nanocomposites prepared from an EVAgMA/50 wt% o-clay masterbatch at a magnification of 250,000. The dark lines represent the silicate layers, and individual silicate layers about 1 nm in thickness can be seen. Figure 4a shows that each layer of the clay was individually and homogeneously dispersed throughout the EVA matrix at the nanometer level. On the other hand, there are some clay layer aggregates at the micrometer level in Fig. 4b. This suggests that incorporation of very large amounts of silicates in the system led to parallel stacking of the silicate layers as well as much stronger flocculation due to the hydroxylated edge-edge interactions between

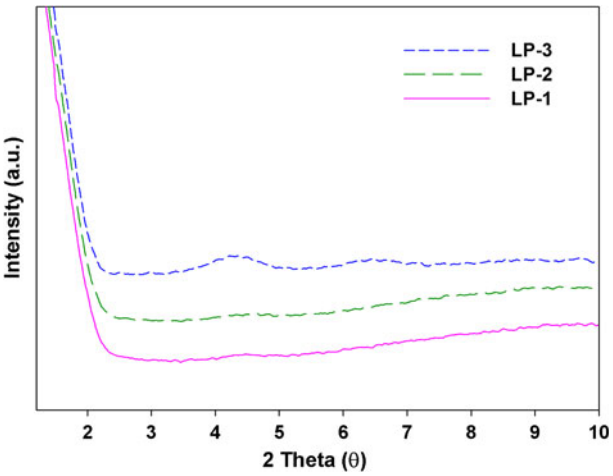

Fig. 3 XRD patterns of EVA/2, 5, 10 wt% o-clay nanocomposites (LP-1 to -3) prepared with an EVAgMA/50 wt% o-clay masterbatch (LMB-3)

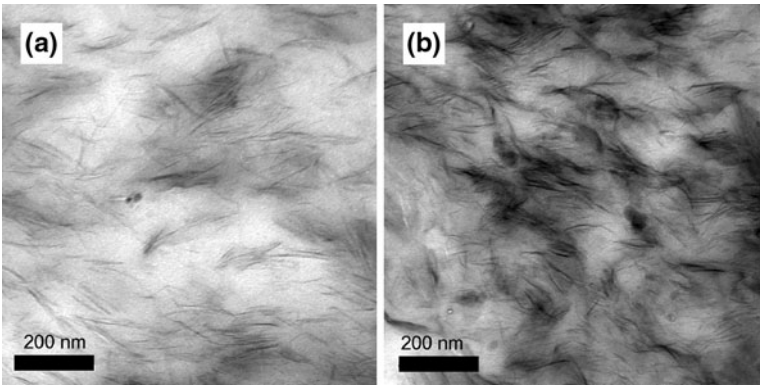

Fig. 4 TEM images of **a** EVA/5 wt% o-clay nanocomposite (LP-2) and **b** EVA/10 wt% o-clay nanocomposite (LP-3) prepared with an EVAgMA/50 wt% o-clay masterbatch (LMB-3)

the silicate layers. Based on these results, we confirmed that the TEM image is in agreement with the X-ray measurements.

Figure 5 shows weight loss curves performed under air for EVA and the EVA/o-clay nanocomposites prepared from an EVAgMA/50 wt% o-clay masterbatch. The TGA curves show that degradation of EVA and the EVA/o-clay nanocomposites occurred in two distinct regions; the first was the loss of acetic acid, followed by the degradation of any remaining unsaturated polyethylene polymer [16]. In general, loss of acetic acid in the nanocomposite was accelerated as a function of the clay content, due to a catalytic effect caused by the acidic sites of the clay [24]. However, it was found that this accelerated elimination of vinylacetate no longer occurred, whereas both degradation steps surprisingly shifted towards higher temperatures. It is also remarkable that nanocomposites with relatively low contents

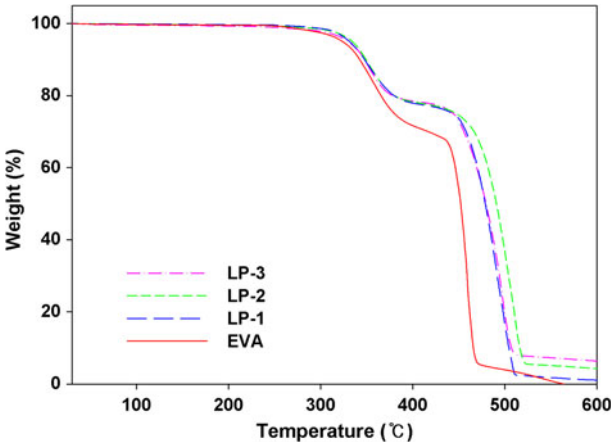

Fig. 5 TGA curves of virgin EVA and EVA/2, 5, 10 wt% o-clay nanocomposites (LP-1 to -3) prepared with an EVAgMA/50 wt% o-clay masterbatch (LMB-3)

of nanoclay (2 and 5 wt%) retarded thermal degradation more than that with high content (10 wt%). Moreover, we confirmed that nanocomposite containing relatively high clay content (5 wt%) within the exfoliated domain generated increased thermal stability. It is thought that the EVAgMA chains anchored to the silicate layers in the masterbatch protect deacylation of EVA from the effects of silicate, while improving dispersion of the clay in the nanocomposite and increasing thermal stability [22]. Therefore, the results should have a beneficial effect on the flame retardant properties of the nanocomposites.

The flammability of neat EVA and the EVA/o-clay nanocomposites fabricated from the EVAgMA/50 wt% o-clay masterbatch were assessed using a cone calorimeter under a heat flux of 50 kW/m^2. In this combustion atmosphere, virgin EVA was characterized by strong bubbling and severe dripping such that we could not confirm the correct experimental result. Thus, Fig. 6a shows the HRRs of only the EVA-based nanocomposites during combustion. For clay loading, up to 10 wt% clay content, are increased in EVA -based nanocomposites, a reduction in the peak HRR of about 40–55% as well as a spread toward a longer period of time were detected. This indicates that the flame retardancy for the EVA-based nanocomposites was strongly dependent on o-clay loading. At the end of combustion, as shown in Fig. 6b, pure EVA was completely burned without any residue. In contrast, EVA-based nanocomposites left a consistent char-like residue. It is also noteworthy that the char-like residue of the nanocomposites was increased and dramatically strengthened with increasing clay content, regardless of the clay dispersion. These results suggest that incorporation of the silicates into nanocomposites during

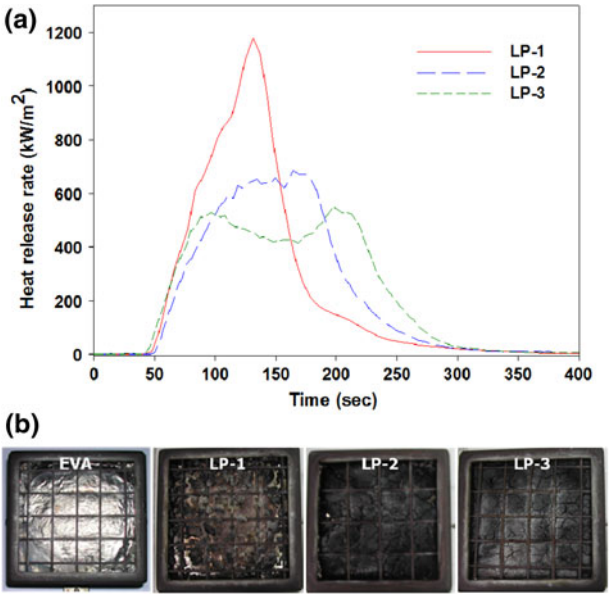

Fig. 6 **a** Heat release rate (HRR) versus time measured with a cone calorimeter (heat flux 50 kW/m^2) for EVA/2, 5, 10 wt% o-clay nanocomposites (LP-1 to -3). **b** Combustion residue images for neat EVA and EVA/2, 5, 10 wt% o-clay nanocomposites (LP-1 to -3)

combustion led to the formation of a catalytic char with high thermal stability that acts as a protective barrier by reducing heat and mass transfer between the flame and polymer. However, the flame retardancy of clay was insufficient since the HRR of clay in the nanocomposites was relatively higher than that typically used in the cable industry, even though clay can improve the flame retardancy of plastics. Therefore, we concluded that clay could be used as a synergistic agent for the improvement of conventional flame retardants such as MDH.

We partially substituted o-clay for MDH by keeping the organic and inorganic contents the same in order to confirm the synergistic flame retardancy of clay in the EVA/MDH composites. Clay as a co-additive was introduced using high clay content EVAgMA/o-clay masterbatch for the preparation of various EVA/o-clay/MDH nanocomposites, the compounding formulations of which are presented in Table 2. As shown in Fig. 7a, the partial substitution of o-clay in place of MDH resulted in dramatic reduction and widening of the HRR compared to those of the EVA/MDH composites (LP-4), as measured by a cone calorimeter (heat flux 50 kW/m^2). The peak HRRs of the EVA/o-clay/MDH nanocomposites were about 45% lower than those of the EVA/MDH composites (LP-4). The HRR curves of the nanocomposites were very similar to each other, but the second peak HRR was comparatively decreased as the o-clay content was increased. In addition, another interesting effect of partially replacing MDH with o-clay was observed by the cohesion of combustion residues. Figure 7b shows the black char-like residues left after the cone calorimeter tests. Numerous cracked crusts were recovered from the

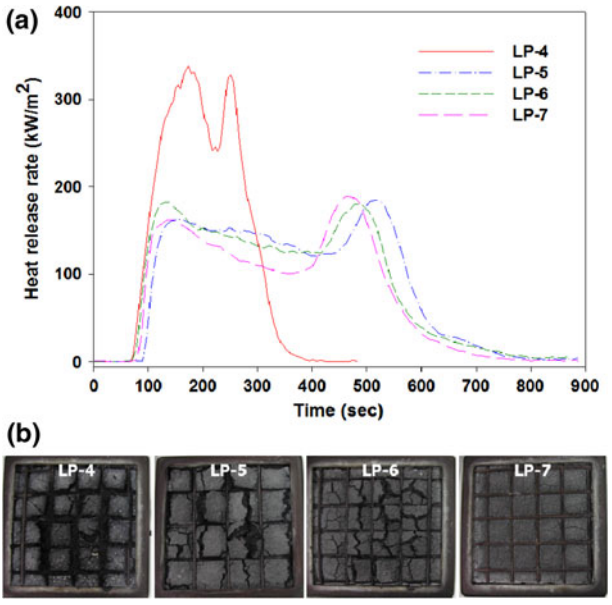

Fig. 7 **a** Heat release rate (HRR) versus time measured with a cone calorimeter (heat flux 50 kW/m^2) for EVA/MDH composite (LP-4) and EVA/o-clay/MDH nanocomposites (LP-5 to -7). **b** Combustion residue images for EVA/MDH composite (LP-4) and EVA/o-clay/MDH nanocomposites (LP-5 to -7)

EVA/MDH composite (LP-4), whereas the EVA/o-clay/MDH nanocomposites (LP-5 to-7) produced uniform and cohesive char-like residues. Considering these results, a small amount of o-clay in place of MDH synergistically increased the flame retardancy. Therefore, the combined condensed-phase and barrier effect between MDH dispersed at the micro-scale level and clay dispersed at the nano-scale level plays a role in directly hindering heat and mass transfer from the flame to the polymer. Therefore, it is believed that the excellent flame-retarded performance of clay as a co-additive in the EVA/o-clay/MDH nanocomposites may decrease the required level of conventional inorganic flame retardant such as magnesium hydroxide and open up a facile route for the fabrication of a new flame retardant system.

Conclusion

In this study, EVAgMA/o-clay masterbatches prepared in a twin-screw extruder with various clay contents up to 50 wt% showed ordered intercalation. The highest clay content EVAgMA/o-clay masterbatch was simply melt compounded with EVA for the preparation of EVA/o-clay nanocomposites containing specific amounts of clay. XRD and TEM confirmed that the clay particles in the EVA/o-clay nanocomposites had fully exfoliated morphologies. This improvement in clay dispersion is attributed to the combination of additional shear force, dilution of polar EVA and similar inherent polarities between the neat EVA and masterbatch. The morphologies of the EVA/o-clay nanocomposites apparently led to both increased thermal properties in air as well as considerably improved flame retardancy. Furthermore, the EVA/o-clay/MDH nanocomposites were also prepared using the high clay content masterbatch in order to confirm the synergistic flame retardancy of clay as a co-additive in the EVA/MDH composites. The HRRs of the EVA/o-clay/MDH nanocomposites prepared by partial replacement of MDH with a small amount of o-clay during combustion were significantly lower and remarkably wider compared to that of EVA/MDH composite. Therefore, these results led us to conclude that the masterbatch approach was very useful for the production of exfoliated EVA/o-clay nanocomposites and for increasing the synergistic flame retardancy of EVA/o-clay/MDH nanocomposites. Consequently, our method is expected to provide a new approach for applying flame retardants to the cable industry.

References

1. Usuki A, Kawasumi M, Kojima Y, Okada A, Kurauchi T, Kamigaito O (1993) Swelling behaviour of montmorillonite cation exchanged for omega-amino acids by epsilon-caprolactam. J Mater Res 8:1174–1178
2. Usuki A, Fukushima Y, Kawasumi M, Okada A, Fukushima Y, Kurauchi T, Kamigaito O (1993) Synthesis of nylon 6-clay hybrid. J Mater Res 8:1179–1184
3. Usuki A, Fukushima Y, Kawasumi M, Okada A, Fukushima Y, Kurauchi T, Kamigaito O (1993) Mechanical properties of nylon 6-clay hybrid. J Mater Res 8:1185–1189

4. Giannelis EP (1996) Polymer layered silicate nanocomposites. Adv Mater 8:29–35
5. Giannelis EP, Krishnamoorti R, Manias E (1999) Polymer-silicate nanocomposites: model systems for confined polymers and polymer brushes. Adv Polym Sci 138:107–147
6. Giannelis EP (1995) Polymer-layered silicate nanocomposites: synthesis, properties and applications. Appl Organomet Chem 12:675–680
7. Gilman JW (1999) Flammability and thermal stability studies of polymer layered-silicate (clay) nanocomposites. Appl Clay Sci 15:31–49
8. Gilman JW, Jackson CL, Morgan AB, Harris R Jr, Manias E, Gianellis EP, Wuthenow M, Hilton D, Philips SH (2000) Flammability properties of polymer layered-silicate nanocomposites. Polypropylene and polystyrene nnocomposites. Chem Mater 12:1866–1873
9. Zanetti M, Kashiwagi T, Falqui L, Camino G (2002) Cone calorimeter combustion and gasification studies of polymer layered silicate nanocomposites. Chem Mater 14:881–887
10. Zanetti M, Camino G, Canavese D, Morgan AB, Lamelas FJ, Wilkie CA (2002) Fire retardant halogen antimony clay synergism in polypropylene layered silicate nanocomposites. Chem Mater 14:189–193
11. Dennis HR, Hunter DL, Chang D, Kim S, White JL, Cho JW, Paul DR (2001) Effect of melt processing conditions on the extent of exfoliation in organoclay-based nanocomposites. Polymer 42:9513–9522
12. Chen JS, Poliks MD, Ober CK, Zhang Y, Wiesner U, Giannelis EP (2002) Study of the interlayer expansion mechanism and thermal-mechanical properties of surface-initiated epoxy nanocomposites. Polymer 43:4895–4904
13. Incarnato L, Scarfato P, Scatteia L, Acierno D (2004) Rheological behavior of new melt compounded copolyamide nanocomposites. Polymer 45:3487–3496
14. Gheysari D, Behjat A (2002) The effect of high energy electron beam irradiation and content of ATH upon mechanical and thermal properties of EVA copolymer. Eur Polym J 38:1087–1093
15. Beyer G (2001) Flame retardant properties of EVA-nanocomposites and improvements by combination of nanofillers with aluminium trihydrate. Fire Mater 25:193–197
16. Zanetti M, Camino G, Thomann R, Mülhaupt R (2001) Synthesis and thermal behaviour of layered silicate-EVA nanocomposites. Polymer 42:4501–4507
17. Zhang W, Chen D, Zhao Q, Fang Y (2003) Effects of different kinds of clay and different vinyl acetate content on the morphology and properties of EVA/clay nanocomposites. Polymer 44: 7953–7961
18. Zanetti M, Camino G, Mülhaupt R (2001) Combustion behaviour of EVA/fluorohectorite nanocomposites. Polym Degrad Stab 74:413–417
19. Jeon CH, Ryu SH, Chang YW (2003) Preparation and characterization of ethylene vinyl acetate copolymer/montmorillonite nanocomposite. Polym Int 52:153–157
20. Riva A, Zanetti M, Braglia M, Camino G, Falqui L (2002) Thermal degradation and rheological behaviour of EVA/montmorillonite nanocomposites. Polym Degrad Stab 77:299–304
21. Tang Y, Hu Y, Wang S, Gui Z, Chen Z, Fan W (2002) Preparation and flammability of ethylene-vinyl acetate copolymer/montmorillonite nanocomposites. Polym Degrad Stab 78:555–559
22. Shi Y, Peterson S, Sogah DY (2007) Surfactant-free method for the synthesis of poly(vinyl acetate) masterbatch nanocomposites as a route to ethylene vinyl acetate/silicate nanocomposites. Chem Mater 19:1552–1564
23. Ray SS, Okamoto K, Okamoto M (2003) Structure-property relationship in biodegradable poly(butylene succinate)/layered silicate nanocomposites. Macromolecules 36:2355–2367
24. Costache MC, Jiang DD, Wilkie CA (2005) Thermal degradation of ethylene–vinyl acetate coplymer nanocomposites. Polymer 46:6947–6958